EMPIRICAL STUDIES OF CROSS-REFERENCE MAXIMUM LIKELIHOOD ESTIMATE RECONSTRUCTION FOR POSITRON EMISSION TOMOGRAPHY

KAO-YIN TU*,***, TAI-BEEN CHEN**, HENRY HORNG-SHING LU**, REN-SHYAN LIU***, KUO-LIANG CHOU***, CHUNG-MING CHEN*****, JYH-CHENG CHEN*

*Institute of Radiological Sciences, National Yang-Ming University, Taipei.
**Institute of Statistics, National Chiao Tung University, Hsinchu
***National PET/ Cyclotron Center, Taipei Veterans General Hospital. Taipei
****Department of Nuclear Medicine, Mackay Memorial Hospital, Taipei
*****Institute of Biomedical Engineering, National Taiwan University, Taipei

ABSTRACT

Positron emission tomography (PET) can reveal subtle metabolic process, which is an important modality for diagnosis. However, spatial resolution of PET images is not as good as computed tomography (CT) or magnetic resonance imaging (MRI), which can show precise anatomical details. Our study is to improve image quality of PET using better reconstruction methods. In this paper, we use a new and efficient method to incorporate the correlated structural information obtained from MRI. A mean estimate smoothing the maximum likelihood estimate (MLE) locally within each region of interest is derived according to the boundaries provided by the structural information. Since the boundaries may not be correct, a penalized MLE using the mean estimate is sought. The resulting reconstruction is called a cross-reference maximum likelihood estimate (CRMLE). The CRMLE is obtained through a modified expectation maximization (EM) algorithm, which is shown to be computationally efficient by our phantom and clinical studies.

Biomed Eng Appl Basis Comm, 2001 (February); 13: 1-7.
Key Words: Maximum likelihood estimate, Expectation maximization algorithm, Positron emission tomography

1. INTRODUCTION

Like X-ray CT, PET images can be reconstructed using filtered-backprojection (FBP) or convolution-backprojection (CBP) algorithms. However, since the FBP algorithm was originally designed for X-ray CT, many assumptions made for the algorithm does not hold for PET image reconstruction. To overcome the problems inherent in the FBP algorithm, various approaches based on maximum likelihood-expectation maximization (ML-EM) algorithms have been proposed, e.g., Shepp and Vardi [1], Lange and Carson [2], Vardi, Shepp and Kaufman [3], Politte and Snyder [4]. The physical process in PET detection may be mod-

Received: Jan. 3, 2001; accepted: Jan. 15, 2001
Address for correspondence: Dr. Jyh-Cheng Chen, Institute of Radiological Sciences, National Yang-Ming University, No.155, Li-Nong St., Sec. 2, Taipei, Taiwan. Tel: 886-2-28267282. Fax: 886-2-28201095. E-mail: jcchen@ym.edu.tw

eled as a Poisson random process. The mean of the observed random variables is indirectly related to the image intensity by a linear transformation. Under this model, there are some sources of errors intrinsic in the reconstruction of PET images. One source of error is caused by the ill-posedness in inverting the linear transformation. Snyder et al. [5] demonstrated that the MLE without regularization shows noises and edges artifacts. A variety of regularization methods have been studied like the Bayesian approaches with different kinds of priors in Hebert and Leahy [6], Green [7], and so on. We have proposed cross-reference methods for reconstructing PET images with prior information [8, 9], which not only fully utilize the correlated structural information to obtain better reconstructions in simulation but also retain the computational efficiency of the ML-EM approach. In this study, we use the CRMLE method, in which we chose the fused images from MRI and PET as the prior information. We show that the method is practically appealing in reconstructing a Hoffman physical phantom and clinical brain images.

2. MATERIALS AND METHODS

There are various estimators, each of which best approximates the unknown parameter to be estimated in a different sense. The first one is the maximum likelihood (ML) estimator, the second and the third one are the maximum a posteriori (MAP) and minimum mean-square-error (MMSE) estimator, respectively [10]. In this study, we use the penalized ML estimator with prior information in penalty to improve PET image reconstruction, which can be regarded as a variant of Bayesian MAP estimators. Our experimental designs are described as follows:

1. We chose MRI images as the source to provide the prior information. We used SIEMENS Vision plus 1.5-T scanner. The scan parameters were TE/TR = 14/500 s, scan matrix = 256 x 256. The data set was acquired from an axial view of a 2D Hoffman brain phantom (see Fig. 1). The phantom was filled with Gd153-DTPA contrast agent. A T1 image was obtained and stored in a DICOM (digital image communication of medicine) format (see Fig. 2).
2. Liquid inside the phantom was emptied and about 3 mCi of ^{18}FDG was injected. Imaging was performed using a Scanditronix PC-4096-15 WB PET scanner with a scan time of 10 min. The PET scans were reconstructed using the convolution back-projection (CBP) method with a matrix size = 128 x 128.
3. The image fusion technique was implemented using the "Interactive Data Language (IDL)" (Research Systems Inc., Boulder, CO). The fusion method was developed in house. The fused image from MRI and PET is shown in Fig. 3.
4. From the fused image we did the image segmentation to extract the useful prior information by a variant of Forgy's method in cluster analysis as explained in Appendix II. The edges between different classes are also displayed that can be used for validation and adjustments.
5. The original sinogram data was used to reconstruct images using MLE-EM and CRMLE-EM, respectively. The differences between the two images were compared by subtraction of these two images.
6. Repeat steps 1~5 with clinical brain data.

Extraction of prior information:

One of the major differences between Bayesian reconstruction and ML-EM method is that Bayesian method takes into account the prior information to improve the estimate (reconstruction) of the parameter of interest, see E. U. Mumcuoglu et al [11], I. T. Hsiao[12] and J. E. Bowsher et al [13]. In this study, we chose the fused image from MRI and PET as the prior information. The MRI image can provide good structural information, while the PET image can provide physiological and metabolic information. Thus, the fused image can contain both anatomical and functional information. In regard to segmentation, we use moving blocks to find the image means and variances in blocks from the fused image with block sizes equal to 2x2, 3x3, 4x4, ..., 128x128. Then, we get a distribution of the variances with respect to different block sizes. The distribution can be approximated by a normal distribution where the mean and standard deviation can be calculated. A variant of Forgy's method in cluster analysis is used to segment the fused image [14].

3. RESULTS

1. 2D Hoffman brain phantom: Fig. 5 shows the fused image of the phantom. Boundaries were extracted from the image to be used as the prior information input to the CRMLE-EM code during the reconstruction (α = 0.0001, with 10 iterations, see Appendix). The image of the prior information is shown in the lower right of Fig. 6, and the reconstructed image by CRMLE-EM is shown in the upper left of Fig. 6. The same data was also reconstructed using the MLE-EM; the reconstructed image is shown in the upper right of Fig. 6. The lower left shows the difference image between the upper two, that is, the CRMLE image substrates the MLE

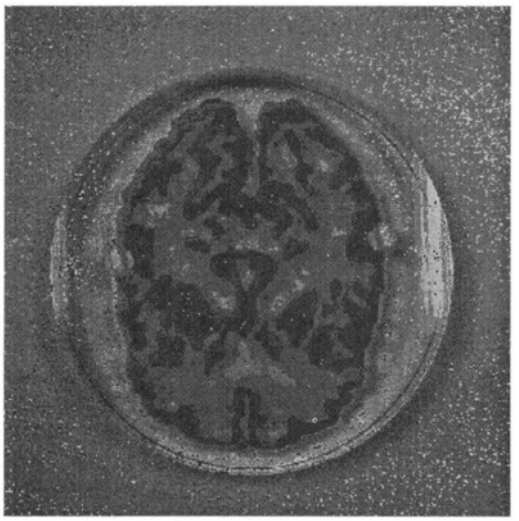

Fig. 1. A 2D Hoffman brain phantom.

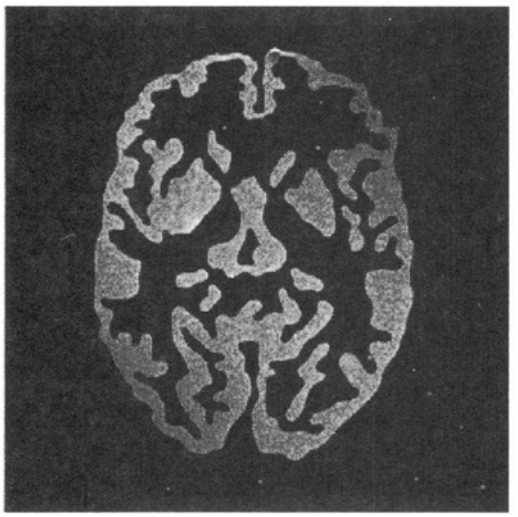

Fig. 2. A 2D Hoffman brain phantom imaged by MRI (SIEMENS Vision plus 1.5T, TE = 500sec, TR = 14sec, T1 Image).

image. Although the images of MLE-EM and CRMLE-EM are similar in visualization, the intensity levels of these two are different so that the difference is as displayed.

2. Clinical brain image: We select a patient whose brain had been scanned by MRI and PET, respectively. We manually selected the corresponding 15 slices from MRI images (see Fig. 7). Using our IDL image fusion code, the 15 fused images were generated as shown in Fig. 8. These 15 fused images were then input to the CRMLE-EM code to get the final reconstructed images as shown in Fig. 9.

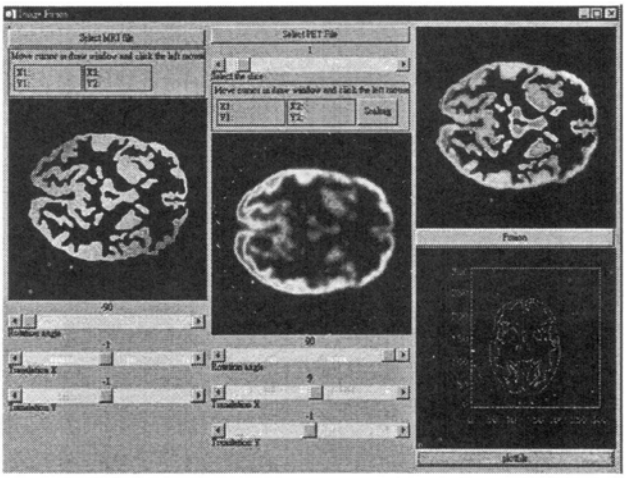

Fig. 3. An in-house image fusion program written in IDL.

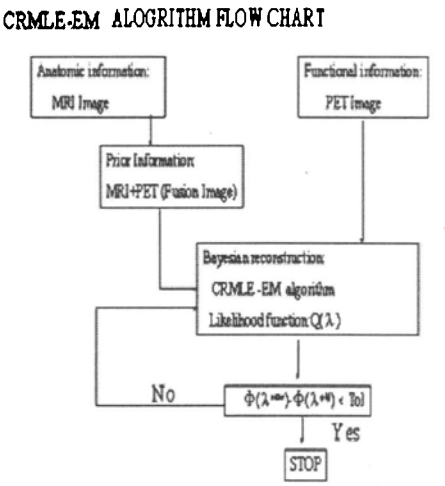

Figure 4: Flow chart of the CRMLE-EM algorithm.

4. DISCUSSIONS

1. The cross-reference methods are quite robust to the mis-registration of boundaries in our previous simulation studies of [8, 9] and current empirical studies.
2. Semi-automatic method by a variant of Forgy's method in cluster analysis is used to segment different regions, which can be improved in the future.
3. From phantom studies, two reconstruction methods were reconstructed at the same iteration numbers: 1, 10, 20, 30, 40, respectively. The CRMLE-EM results are shown in the first row of Fig. 10 (A), and the MLE-EM results are shown in the second row of Fig. 10 (A). We see that CRMLE-EM contains more structural information than MLE-EM does.

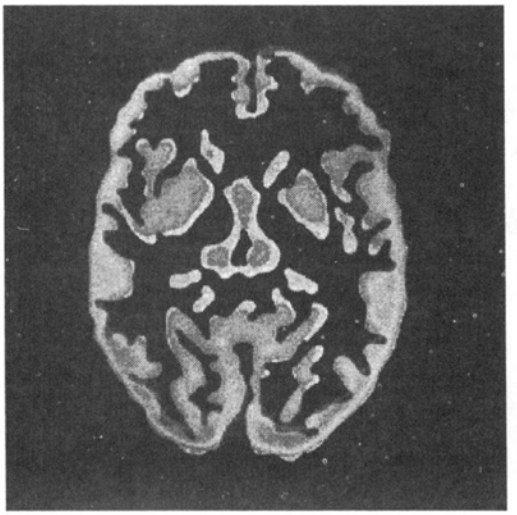

Fig. 5. Fused image of PET and MRI images of the 2D Hoffman brain phantom.

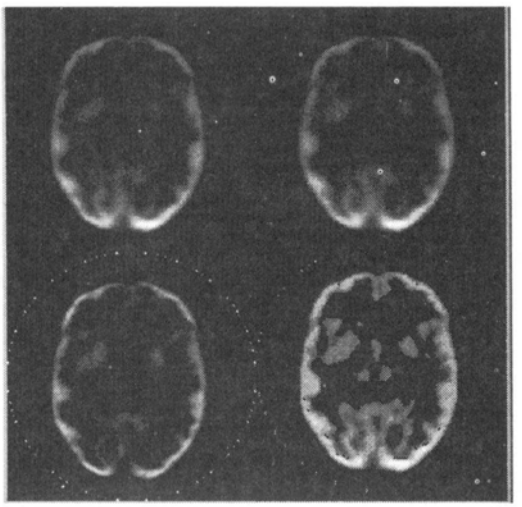

Fig. 6: Reconstructed image with CRMLE-EM and MLE-EM algorithms. The upper left is the CRMLE-EM reconstructed image, and the upper right is the MLE-EM reconstructed image. The difference of the CRMLE image subtracts the MLE image is displayed in the lower left and the prior information image is shown on the lower right.

The difference images (CRMLE-EM images - MLE-EM images) are shown in the third row of Fig. 10 (A). At the 10th iteration, the difference is obvious, especially in the boundary. As the iteration number increases, the differences about structural information remain. The fourth row of Fig. 10 (A) shows the image of the prior information used in CRMLE-EM reconstruction. The above steps are repeated for the clinical studies and the results are shown in Fig. 10 (B). We see that the images of the CRMLE-EM results contain more structural information. Their differences are shown in the third row of Fig. 10 (B), where the differences in structural information remain. Although the images of MLE-EM and CRMLE-EM are similar in visualization, the intensity levels of these two are different so that the difference is as displayed.

4. For objective assessment of image quality of the two methods, receiver operating characteristic (ROC) curve analysis will be studied in the future.

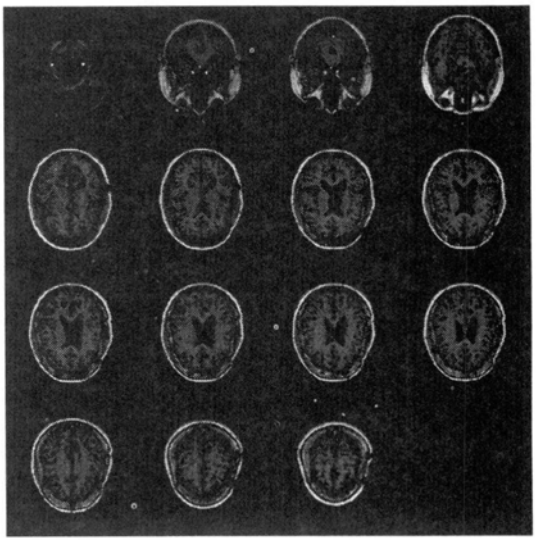

Fig. 7: MRI images of a clinical brain.

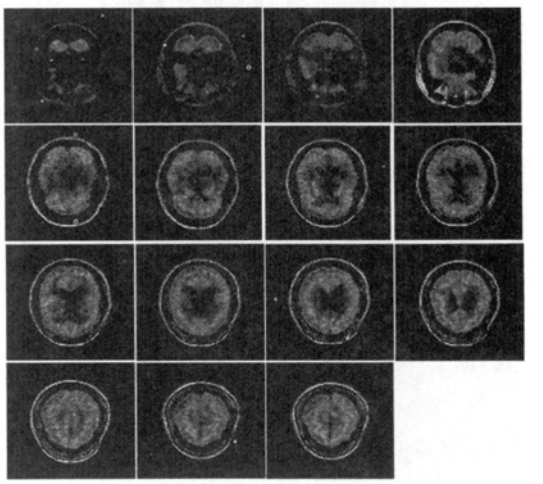

Fig. 8. Fused images of PET and MRI images of the brain.

5. CONCLUSIONS AND FUTURE WORKS

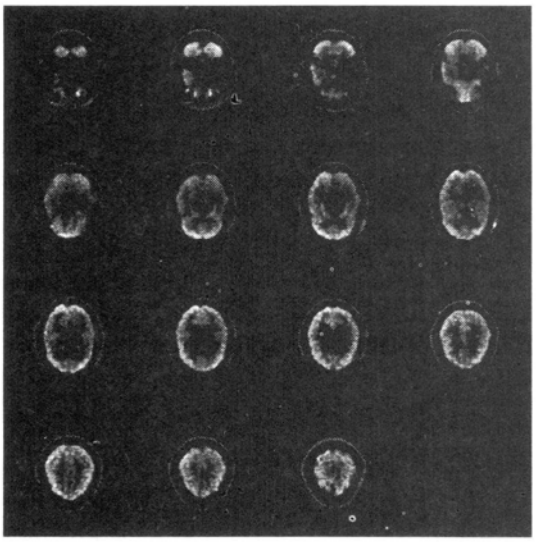

Fig. 9. CRMLE-EM reconstructed image (clinical brain image).

It has been shown in this study that the proposed CRMLE may take advantage of prior information effectively (even in the case of incorrect boundary information). The phantom and clinical studies demonstrate the improvements of the CRMLE over the MLE on real PET images. While our current results have confirmed that the CRMLE is a promising approach, further studies are definitely required to make this scheme clinically applicable. We are interested in pursuing further topics including the acceleration of algorithm, automatic image segmentation method, and quantity analysis of image quality of the reconstructed images by clinical diagnostic values.

ACKNOWLEDGMENTS

This work was supported in part by the National Science Council and Atomic Energy Council of Taiwan under grant NSC 89-NU–7-010-002. Specific thanks to Ruey-Ming Huarng for help in MRI phantom acquisition.

REFERENCES

1. Shepp LA and Vardi Y: Maximum likelihood reconstruction for emission tomography. IEEE Trans Med Imaging 1982; vol. MI-1: 113-122.
2. Lange K and Carson R: EM reconstruction algorithms for emission and transmission Tomography. J Comput Assist Tomog 1984; 8: 306-316.
3. Vardi Y, Shepp LA and Kaufman L: A statistical model for positron emission tomography. Journal of the American Statistical Association 1985; 80: 8-20.
4. Politte DG and Snyder DL: Corrections for accidental coincidences and attenuation in maximum-likelihood image reconstruction for positron-emission tomography. IEEE Trans Med Imaging 1991; 10: 82-89.
5. Snyder DL, Miller MI, Thomas LJJ and Politte DG:

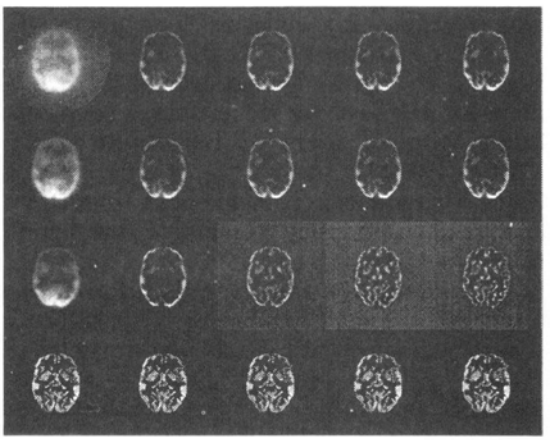

Fig. 10 (A)

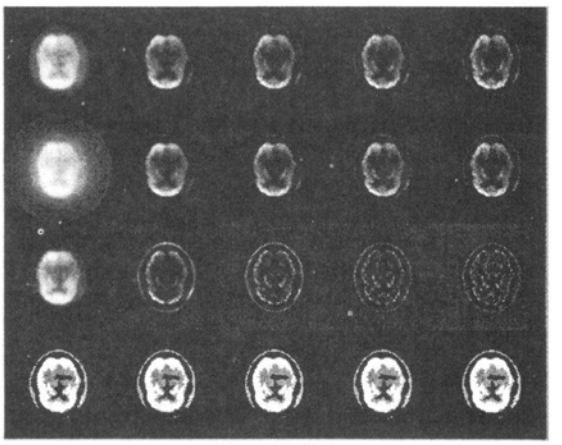

Fig. 10 (B)

Fig. 10. (A) 2D Hoffman brain phantom study: The first row contains the CRMLE reconstructed images, with α = 0.0001, at different iteration number (1,10,20,30,40,50). The second row contains the MLE-EM reconstructed images at different iteration number (1,10,20,30,40,50). The third row contains the difference images (CRMLE-EM images subtract MLE-EM images). The last row contains the images of the prior information used, which are the same at all iterations.
(B) Clinical brain image study: Same display setup as in (A) is used here except that the phantom is replace by the clinical brain data.

Noise and edge artifacts in maximum-likelihood reconstructions for emission tomography. IEEE Trans Med Imaging 1987; 6: 228-238.
6. Hebert T and Leahy RM: A generalized EM algorithm for 3D Bayesian reconstructon from poisson data using gibbs priors. IEEE Trans Med Imaging 1989; 8: 194-202.
7. Green PJ: Bayesian reconstructions from emission tomography data using a modified EM algorithm. IEEE Trans Med Imaging 1990; 9: 84-93.
8. Lu HHS, Chen CM and Yang IH: Cross-reference weighted least square estimates for positron emission tomography. IEEE Trans Med Imaging 1998; 17: 1-8.
9. Lu HHS and Tseng WJ: On accelerated cross-reference maximum likelihood estimates for positron emission tomography. IEEE Nuclear Science Symposium 1997; 2: 1484-1488.
10. Dougherty ER: Random processes for image and signal processing. SPIE/IEEE Express, USA, 1999; 72-90.
11. Mumcuoglu EU, Leahy RM and Cherry SR: Bayesian reconstruction of PET images: methology and performance analysis. Phys Med Biol 1997; 42: 1777-1807.
12. Hsiao IT: Bayesian Imaging reconstruction for emission and transmission tomography. PhD Dissertation, State University of New York at Stony Brook, 2000.
13. Bowsher JE, Johnson VE, Turkington TG, Jaszczak RJ, Floyd CE and Coleman RE. Bayesian reconstruction and use of anatomical a priori information for emission tomography. IEEE Trans Med Imaging 1996; 15: 673-686.
14. Kaufman L and Rousseeuw PJ. Finding groups in data: an Introduction to cluster analysis. John Wiley & Sons Inc, New York, USA, 1990; 112.

Appendix

I. The GEM Algorithm for CRMLE:

According to the notations and setups in [1, 3], the observed log-likelihood function in the incomplete space is

$$l(\lambda) = \sum_{d=1}^{D}\{\sum_{b=1}^{B} n^*(d)\ln[\lambda^*(d)] - \lambda^*(d)\} + \text{constant}.$$

The CRMLE-EM can be derived as follows.

$$\hat{\lambda}_{CRMLE} = \arg\min_{\lambda\ge 0}\Phi(\lambda),$$

where

$$\Phi(\lambda) = -l(\lambda) + \alpha\|\lambda - \hat{\lambda}_{MEAN}\|^2 \quad ,$$

$\alpha > 0$, λ_{MEAN} is the local average of the MLE within every segmented region and 2-norm is used. Hence,

$$\text{if } \alpha \to 0, \text{ then } \hat{\lambda}_{CRMLE} \to \hat{\lambda}_{MLE}.$$

$$\text{If } \alpha \to \infty, \text{ then } \hat{\lambda}_{CRMLE} \to \hat{\lambda}_{MEAN}.$$

The Lagrangian function can be obtained after introducing the Largrangian multipilier, $\beta = (\beta(1),..., \beta(B))$,

$$\Psi = -l(\lambda) + \alpha\|\lambda - \hat{\lambda}_{MEAN}\|^2 - \beta^T\lambda$$

The Kuhn-Tucker (KT) can be applied accordingly. Also, the modified EM algorithm in [7] can be applied as follows. The E-step without constant terms becomes

$$\begin{aligned} &Q(\lambda^{new}\,|\,\lambda^{old}) - \alpha\|\lambda^{new} - \hat{\lambda}_{MEAN}\|^2 \\ &= -\sum_d\sum_b p(b,d)\lambda^{new}(b) \\ &\quad + \sum_d\sum_b \log\{p(b,d)\lambda^{new}(b)\}n^*(d)\frac{p(b,d)\lambda^{old}(b)}{\sum_{b'=1}^{B}p(b',d)\lambda^{old}(b)} \\ &\quad - \alpha\|\lambda^{new} - \hat{\lambda}_{MEAN}\|^2 \end{aligned}$$

The M-step solves

$$\frac{\partial\{Q(\lambda^{new}\,|\,\lambda^{old}) - \alpha\|\lambda^{new} - \hat{\lambda}_{MEAN}\|^2\}}{\partial\lambda^{new}(b)} = 0.$$

Hence,

$$\frac{\hat{n}(b,\cdot)}{\lambda^{new}(b)} - \sum_{d=1}^{D} p(b,d) - 2\alpha[\lambda^{new}(b) - \hat{\lambda}_{MEAN}(b)] = 0,$$

where

$$\hat{n}(b,\cdot) = \lambda^{old}(b)\sum_{d=1}^{D}\frac{p(b,d)n^*(d)}{\sum_{b'=1}^{B}p(b',d)\lambda^{old}(b')}$$

That is,

$$A[\lambda^{new}(b)]^2 + B\lambda^{new}(b) - C = 0,$$

where

$$A = 2\alpha,$$

$$B = p(b,\cdot) - 2\alpha\hat{\lambda}_{MEAN}(b), p(b,\cdot) = \sum_{d=1}^{D} p(b,d),$$

$$C = \hat{n}(b,\cdot),$$

So, the unique nonnegative solution turns out to be

$$\lambda^{new}(b) = \frac{-B + \sqrt{B^2 + 4AC}}{2A}$$

The resulting modified EM algorithm can be stated as follows.
Choose initial values $\lambda^{old}(b) > 0$, b = 1, 2, 3,..., B.
Compute a new estimate $\lambda^{new}(b)$ for b = 1, 2, 3,..., B.
If $\Phi(\lambda^{new}) - \Phi(\lambda^{old})$ is smaller than a tolerance, then stop.
Otherwise, go to step 2 with λ^{old} replaced by λ^{new}.

II. The Algorithm for segmentation:

Let Y_j be the intensity of jth pixel of a NxN image, which is assumed to be a random variable following a normal distribution. The N-1 sequences of

block means with different block sizes, from 2x2, 3x3, ..., NxN, are obtained. Then, the maximum and minimum values of all sequences are calculated, which are denoted as M and m, respectively. The standard deviation of the entire image is computed and is denoted as S. Suppose that the whole image has K partitions, $C_1,...,C_K$, and the following algorithm is applied. A variant of Forgy's method in cluster analysis is used Step 1 and 2 (e.g., see pp. 112 in [14]).

Algorithm Steps:

Initialization:

The mean of ith partition is set by $\mu_i^{(0)} = m + i(M-m)/K, i = 1,2,...,K.$

The stander deviation of ith partition is set equally by $\sigma_i^{(0)} = S, i = 1,2,...,K.$

The iteration number l is set to be 0.

Clustering:

The iteration number is incremented by 1, $l = l+1$. For each pixel, it is classified into a class that has the maximum probability. That is, $Y_j \in C_i^{(l)}$, where $i = \arg\max P_{\mu_k^{(l)},\sigma_k^{(l)}}(Y_j)$ and $C_i^{(l)}$ is the class index set at current iteration. Let $n_i^{(l)}$ be the numbers of $C_i^{(l)}$. If $n_i^{(l)}$ equal to zero for some i, then ith class is deleted and rearrange the partition index.

Updating:

The mean and stander deviation of each class is updated by

$$\mu_i^{(l)} = \frac{\sum_{j \in C_i^{(l)}} Y_j}{n_i^{(l)}}, \quad \sigma_i^{(l)^2} = \frac{\sum_{j \in C_i^{(l)}} (Y_j - \mu_i^{(l)})^2}{n_i^{(l)} - 1}, \quad where\ i = 1,2,\cdots,K.$$

Stopping:

If $|\hat{\mu}_i^{(l)} - \hat{\mu}_i^{(l-1)}| < \varepsilon_1$, and $|\hat{\sigma}_i^{(l)^2} - \hat{\sigma}_i^{(l-1)^2}| < \varepsilon_2, \forall i,$ then stop.

Else, $l=l+1$ and go to step 2.